JOURNAL OF IRON AND STEEL RESEARCH, INTERNATIONAL. 2014, 21(10): 938-944

Shear Fracture of Advanced High Strength Steels

Sheng HUANG[1], Yi-xi ZHAO[2], Chun-feng HE[1]
(1. State Key Laboratory of Mechanical System and Vibration, Shanghai Jiao Tong University, Shanghai 200240, China; 2. Shanghai Key Laboratory of Digital Manufacture for Thin-walled Structures, Shanghai Jiao Tong University, Shanghai 200240, China)

Abstract: Failure experiments were carried out through a stretch-bending test system for advanced high strength steels, i. e. dual-phase (DP) steels and martensitic steels (MS). The die radius in this system was designed from 1 to 15 mm to investigate the failure mode under different geometries. Two failure modes were observed during the experiments. As a result, critical relative radii (the ratio of inner bending radius R to sheet thickness t) for DP590 and DP780 steels were obtained. The stretch-bending tests of DP980 display some trends unlike DP590 and DP780 steels, and curve of DP980 in different thicknesses does not coincide well. High blank holder force exhibits more possibility of shear fracture tendency than low blank holder force. The unique character of high strength martensitic steel (1500MS) is that no shear fracture is found especially over small bending radius ($R=2$ mm) under the same experimental conditions. Microstructure analysis indicates that there are obviously elongated grains on shear fracture surface. It shows smaller diameter and shallower depth of the dimples than the necking failure.

Key words: advanced high strength steel; shear fracture; critical R/t; blank holder force; microstructure

Lightweight materials such as advanced high strength steels (AHSS) have been increasingly used in the automotive industry for the requirements of both high strength and weight reduction[1]. Comparing with conventional steels, AHSS have higher strength and lower formability. The application of AHSS has met many challenges, such as early fracture, high springback, edge cracking, high residual stress, die wear, and high load capacity for press[2]. So a smaller die radius is used in the mold design, and blank holder force (BHF) is increased in the process. Among the defects, the early fracture is referred to as shear fracture by the automotive industry. This is due to the fracture occurring along maximum shear planes which are positioned at 45° to the principal directions of deformation[3]. Shear fracture is significantly different from the necking failure of conventional steels. It occurs parallel to and near the die, under both stretching and bending stress states. Shear fracture is a feature unique to AHSS, without obvious thinning and necking[4].

Li et al.[5] discovered that the traditional forming limit diagram (FLD) theory based on necking instability cannot predict the shear fracture under stretch bending over small radius. Shear fracture occurs earlier than the FLD predicts, and the ultimate strain of the material at fracture does not reach the strain on forming limit curve (FLC). Kim et al.[6] studied the shear fracture of dual-phase steel, and they believed that the shear fracture is caused by the temperature and has nothing to do with the microstructure.

In the present work, characteristics of stretch-bending fracture in AHSS over small die radius were investigated through a stretch-bending test system. With the help of optical metallographic microscope and scanning electron microscope (SEM), the fracture surface and the undeformed surface were observed and compared.

1 Experimental Procedure

1.1 Material properties

Two kinds of AHSS were investigated in the

Foundation Item: Item Sponsored by National Natural Science Foundation of China (51075267); International Cooperation Program in Science and Technology of MOST of China (2010DFA72760)
Biography: Sheng HUANG, Doctor Candidate; **E-mail**: hsheng@sjtu.edu.cn; **Received Date**: May 7, 2013
Corresponding Author: Yi-xi ZHAO, Doctor, Associate Professor; **E-mail**: yxzhao@sjtu.edu.cn

experimental procedure: one kind is dual-phase (DP) steels and the other is martensitic steel (MS).

DP steels are by far the most popular AHSS alloys, which account for 75% of the total sheet material used in the program of UltraLight Steel Auto Body-Advanced Vehicle Concepts (ULSAB-AVC)[7,8].

The strengthening method of AHSS is mainly phase transformation, and martensite is the strengthening phase. MS steel[9] is another kind of AHSS characterized of very high strength with small amount of ferrite in a large matrix of martensite. The maximum ultimate tensile strength of MS steel is up to 1700 MPa due to the large volume fraction of martensite.

The engineering stress-strain curves of these materials shown in Fig. 1 are gained by the standard uniaxial tensile tests according to Chinese standard GB/T 228-2010 (ASTM E8). In the table of mechanical properties (Table 1), n stands for the strain hardening exponent and K stands for the hardening coefficient. n and K are fitting in accordance with Hollomon relationship.

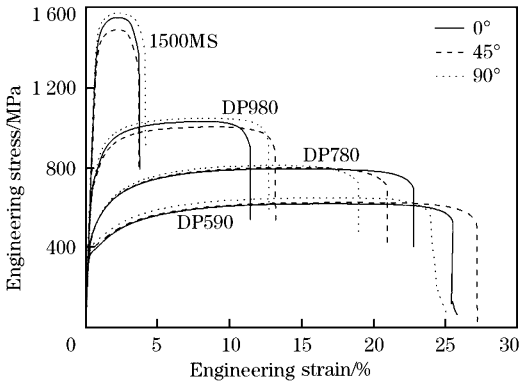

Fig. 1 Engineering stress-strain curves

Table 1 Mechanical properties of sheets

Steel grade	DP590	DP780	DP980	1500MS
Yield strength/MPa	384	461	716.3	1467.1
Ultimate tensile strength/MPa	628	802	1027	1566.9
Total elongation/%	26.4	20.7	7.4	2.4
n	0.16	0.13	0.11	0.08
K/MPa	986	1164	1479.2	2199.1

1.2 Stretch-bending tests of AHSS

A newly designed stretch-bending test system with data acquisition device is introduced for the experiments of AHSS. Fig. 2 is the design of the stretch-bending test system. The die is changeable with a radius of 1, 2, 4, 6, 8, 10, and 15 mm, respectively. BHF can be adjusted by the press from 0 to 300 kN. The rectangle sheet specimen with size of 250 mm×40 mm is used in the experiments.

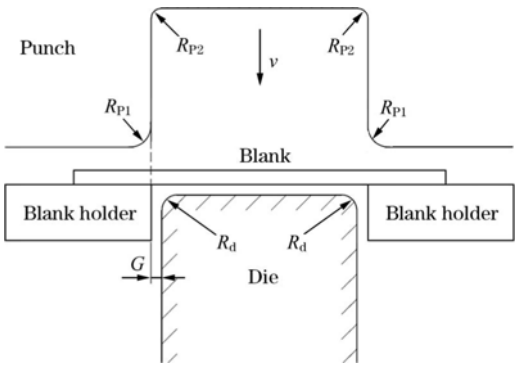

R_{P1}=16 mm; R_{P2}=3.5 mm; R_d=Variable; G=1.75 mm.

Fig. 2 Sketch of stretch-bending test system

During the experiment, punch and blank holder clamped the sheet specimen and moved downward at 10 mm/s, the sheet specimen stayed stationary to the punch, but the die was against the movement. With the increase of forming depth, a groove-shape specimen was formed. The die reaction force and forming depth were recorded during this process. Die reaction force increases with the increase of forming depth. When the die force reached maximum value, the experiment stopped since the specimen cracked.

Shear fracture of DP steels occurs over small radius in stretch-bending experiments. In order to increase the flow resistance, two draw-beads were used in the stretch-bending experiments over different radius.

BHF is also an important factor in sheet forming process. The sheet specimen suffered both stretch stress and bending stress with the friction and deformation against the die fillet. BHF affects the friction, which causes the stretch stress in sheet specimen. Bending stress is decided by the die radius. Thus, the BHF actually reflects the ratio of stretch to bending. The schematic illustration of deformed sheet in stretch bending in Fig. 3 shows the effects of stretch and bending.

2 Results and Discussion

2.1 Stretch-bending test results of AHSS

2.1.1 Radius

Fig. 4 is the forming depth versus die reaction force curves for DP590 and DP780 steels. When R is a small value, the maximum die reaction force increases as the radius increases, and the fracture mode is shear fracture. After the R reaches a certain

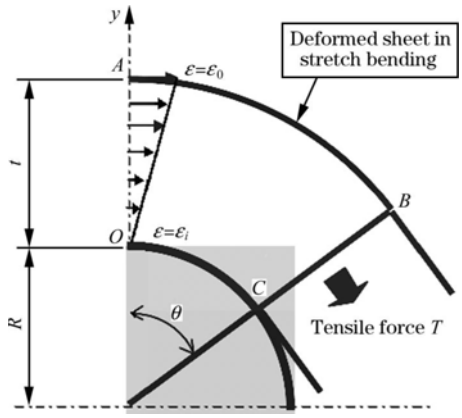

Fig. 3 Schematic illustration of deformed sheet in stretch bending

value and keeps increasing, maximum die reaction force stays at a constant value. The fracture mode in DP steel transfers into necking failure. This certain relative radius R/t value at transition is regarded as the critical R/t value of shear fracture under stretch bending. The processing of data is presented in Fig. 5.

The critical R/t values for DP590 and DP780 steels are 3.89 and 5.56, respectively. It can be concluded that the higher the strength of DP steel is, the more easily the shear fracture occurs. For example, when $R/t=4.8$, the fracture mode of higher strength DP780 steel in the stretch-bending test is shear fracture, but under the same condition, the fracture mode of the lower strength DP590 steel is still necking failure. DP780 steel is much easier to fail as shear

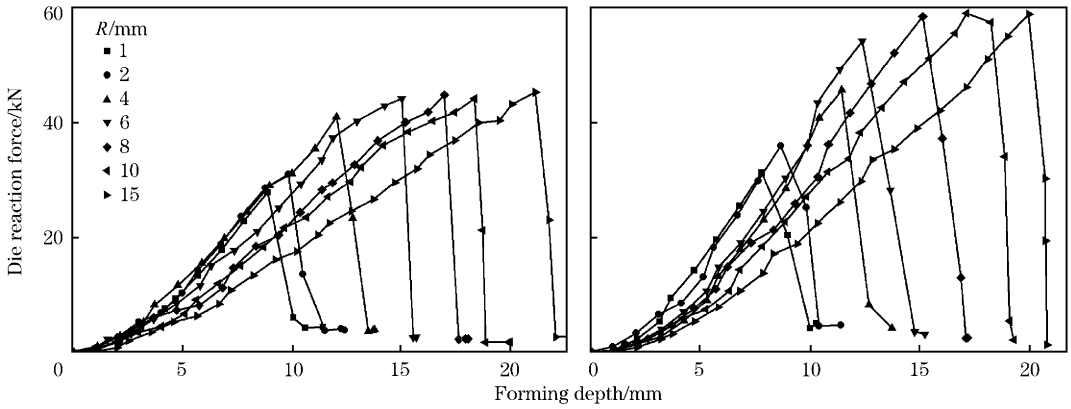

Fig. 4 Die reaction forces in stretch-bending tests of DP590 and DP780 steel

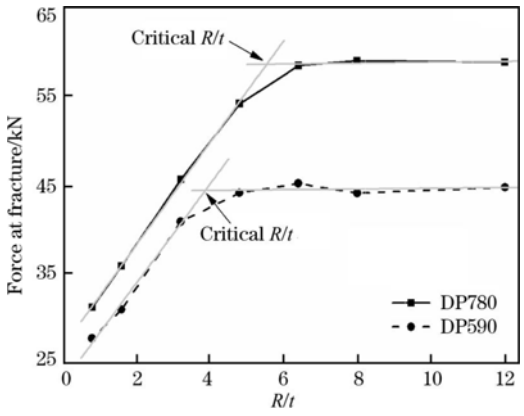

Fig. 5 Critical R/t value

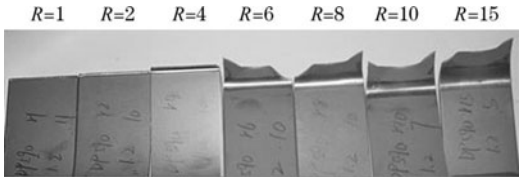

Fig. 6 Fracture modes and location of DP590 steel over different die radii ($t=1.2$ mm)

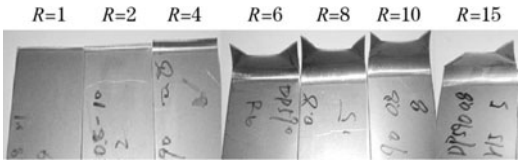

Fig. 7 Fracture modes and location of DP590 steel over different die radii ($t=0.8$ mm)

fracture than DP590 steel.

With the increase of relative radii, the failure position will change from the fillet to the wall. Figs. 6 and 7 are the fracture modes and failure location of DP590 steel over various die radii. Fig. 8 shows the failure sample of DP780 steel, where t is the sheet thickness. It implies that shear fracture appears without obvious thinning and necking at the fracture surface compared to necking failure. The thinning rates of fracture surface (DP780 steel, $t=1.25$ mm) are shown in Table 2.

For DP980 steel, shear fracture also occurred during the experiment. The relationship between die reaction force at fracture and die radius is present in

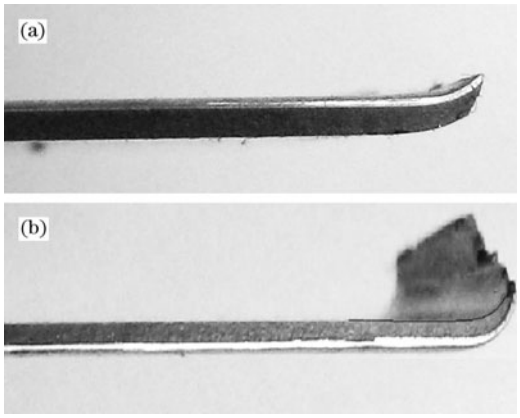

(a) Shear fracture; (b) Necking failure.

Fig. 8 Fracture sample of DP780 steel (t=1.25 mm)

Table 2 Thinning rate of fracture surface (DP780 steel, t=1.25 mm)

R/t	R/mm	Thinning rate/%
1.6	2	2.97
4.8	6	5.02
8.0	10	30.56

Fig. 9. As the die radius increases, the maximum die reaction force at fracture of DP980 steel increases at the beginning, and then decreases. This is not similar to DP590 and DP780 steels, where the maximum die reaction force at fracture increases at first, then keeps a constant value.

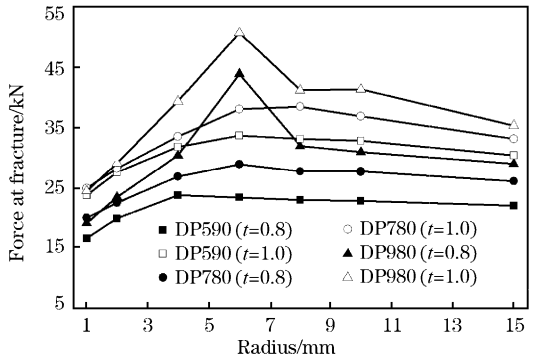

Fig. 9 Different force trends of DP980 steels

2.1.2 Thickness

Thickness of 0.8 and 1.0 mm of DP steels were selected during the experiments. Maximum die reaction force in each experiment depends on the strength of sheet, and higher strength sheet surely results in higher die reaction force. Normalized die reaction force at fracture (the ratio of die reaction force to maximum die reaction force at fracture) is used as the Y-axis for comparability and consistency, as shown in Fig. 10. The results suggest that as the thickness changes, the relative radii R/t for DP590 and DP780 steel sheets coincides well, which means there is little difference between different thicknesses, and the critical R/t value can be used as a criterion for shear fracture of DP590 and DP780 steels. The curve of DP980 steel in different thicknesses does

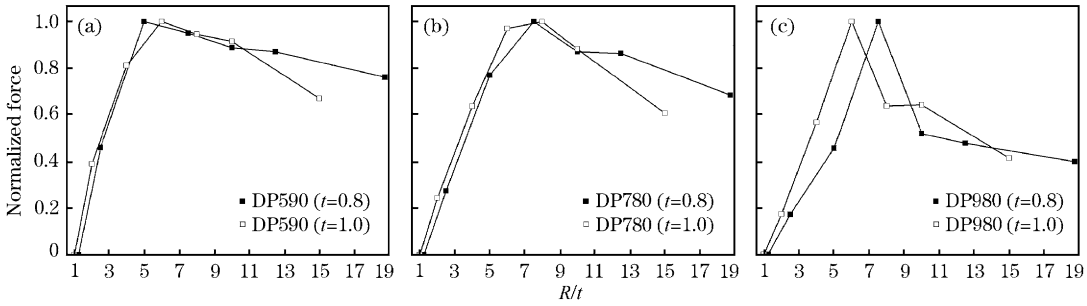

Fig. 10 Relationship between normalized force and relative radius

not coincide with that of the DP590 and DP780 steels, especially when the radius is 4 mm. There is an obvious offset from one to another, and trend lines in Fig. 5 cannot be obtained with DP980 steel.

The strength grade of DP steel is controlled by the volume fraction of martensite[10]. Luo et al.[11] reported that the volume fraction of martensite in DP590 steel is about 18%, and in DP780 steel it is about 30%, while in DP980 steel it is up to about 52%. Maybe these differences of DP980 steel are due to the increase of yield strength and ultimate tensile strength[12], and the volume fraction of martensite in DP980 steel is larger which exceeds the half of total.

2.1.3 BHF

Fig. 11 is the final specimens under various BHFs. With the increase of BHF, the fracture location of specimen transfers from the sidewall to the tangent of the sidewall with bending fillet, and to the fillet of die gradually. Fracture under low BHF with thinning and necking on the sidewall is obviously necking failure,

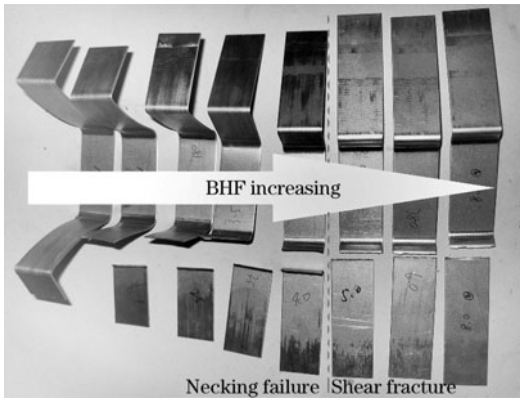

Fig. 11 Forming results under different BHFs

while the fracture mode at the fillet of die is shear fracture.

2.1.4 Material type

In the stretch-bending experiments of 1500MS steel, the BHF was set to 300 kN, and the die radius was 2 mm. Fig. 12 is the comparison of DP590, DP780 and 1500MS specimens. Under the same conditions, DP590 and DP780 steels were cracked, but the 1500MS steel did not. Other experiments showed that 1500MS steel also did not crack when the die radius was larger than 2 mm. Result of high strength MS steel reveals that it has special features on stretch-bending tests over small die radius compared with DP steels, although the volume fraction of martensite is much larger than that in the DP steels. MS steel shows better bendability. No shear fracture is found under small bending radius ($R=2$ mm) even though the process conditions are the same.

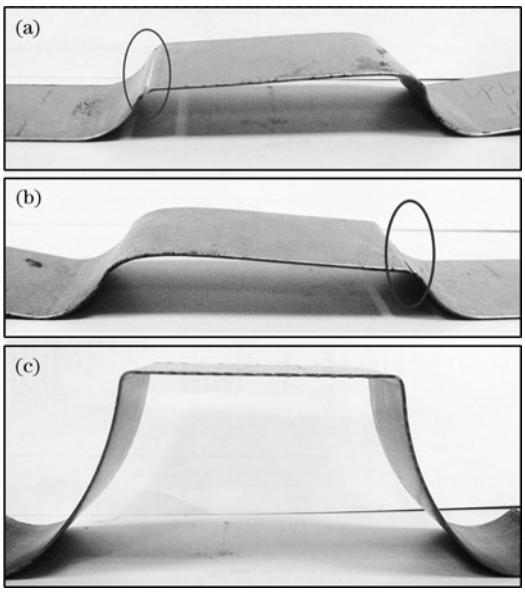

(a) DP590, cracked; (b) DP780, cracked; (c) 1500MS, not cracked.

Fig. 12 Results of MS steel

The bending stress takes the leading role in the stretch-bending tests when the radius is small. MS steel has better bendability, which leads to the result of no cracking.

2.2 Microstructure on specimens of shear fracture

The fracture specimens were cut, mechanically polished and etched in 4% Nital solution for 10—15 s to observe the microstructure of fracture. Fig. 13 shows the observation location of shear fracture specimens by optical metallographic microscope, which includes the fracture surface view (direction 1) and undeformed surface view (direction 2).

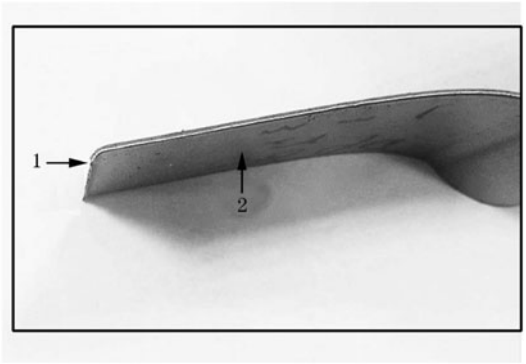

Fig. 13 Microstructure observation

Fig. 14 shows the micrograph of shear fracture specimens (DP780 steel, $R=2$ mm) by optical metallographic microscope. The white part is ferrite phase, while the gray part is martensite phase. Martensite phase is distributed in the ferrite matrix dispersedly. After deformation, there are obviously elongated grains along the stretch direction on the fracture surface view (Fig. 14(a)), while microstructure of the undeformed surface view (Fig. 14(b)) is relatively uniform.

Fig. 15 shows the micrograph of shear fracture specimen (DP980 steel, $R=2$ mm). The volume fraction of martensite phase in DP980 steel (gray part) is larger than that in DP780 steel (Fig. 14), and the martensite phase of the undeformed surface (Fig. 15(b)) shows a more continuous mesh shape. After deformation under the same condition, the elongation of grains at shear fracture surface (Fig. 15(a)) appears to be more obvious than that in DP780 steel (Fig. 14(a)).

To identify the surface morphology of fracture, samples were observed by SEM. In Fig. 16, both the shear fracture and the necking failure are of mainly ductile fracture with dimple appearance. Figs. 16(a), 16(b)

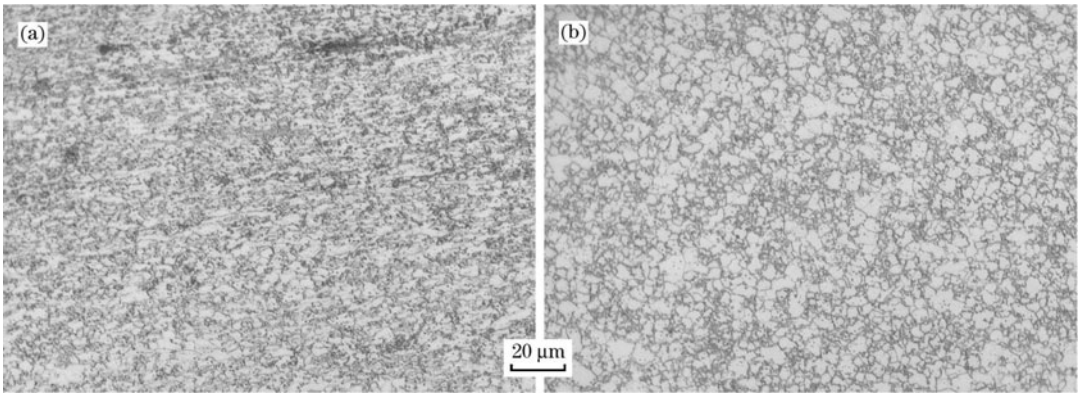

(a) Fracture surface; (b) Undeformed surface.

Fig. 14 Microstructure of DP780 steel

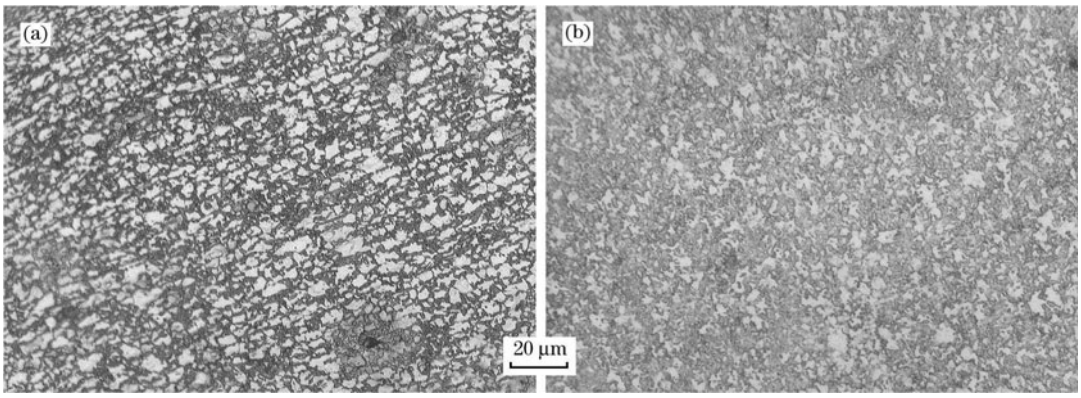

(a) Fracture surface; (b) Undeformed surface.

Fig. 15 Microstructure of DP980 steel

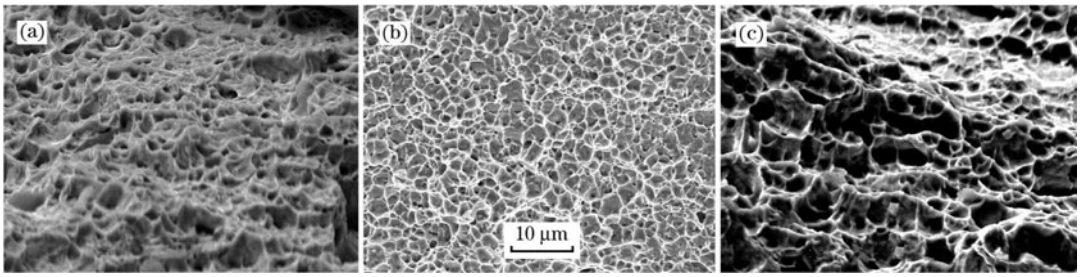

(a) DP590 steel, shear fracture; (b) DP780 steel, shear fracture; (c) DP590 steel, necking failure.

Fig. 16 Fracture microstructure of steels

and 16(c) are under the same magnification, but the shear fracture shows smaller diameter and shallower depth of the dimples than the necking failure. The shear fracture is mainly because the material cleavage fracture occurred despite a large number of dimples exist in the plastic deformation process, while the necking failure is mainly due to the growth and coalescence of dimples under tensile stress.

3 Conclusions

(1) As the relative radius decreases, the failure mode in DP transfers from necking failure to shear fracture. The failure position will change from the wall to the fillet with the transfer from necking failure to shear fracture, which exhibits little thinning and necking near the fracture.

(2) For DP590 and DP780 steels, the R/t has an influence on the fracture mode, while for DP980 steel, the curve in different thicknesses does not coincide with that of the DP590 and DP780 steels.

(3) The failure mode is also affected by the blank holder force parameters. With the increase of BHF, the failure mode in DP steels transfers from tensile fracture to transitional fracture, and then to

shear fracture gradually.

(4) Martensitic steel has special features on tensile stretch forming over small die radius compared with DP steels. No shear fracture is found under small bending radius ($R=2$ mm) even though the process conditions are the same.

(5) There are obviously elongated grains on the fracture surfaces after fracture. The shear fracture shows smaller diameter and shallower depth of the dimples than the necking failure.

References:

[1] Z. W. Wang, N. Zhang, J. Iron Steel Res. Int. 18 (2011) Suppl.1-2, 747-751.

[2] M. Y. Demeri, ASM Handbook: Metalworking: Sheet Forming, V. 14B: Materials Park, ASM International, OH, USA, 2006.

[3] M. P. Sklad, in: Pavel Hora (Eds.), Numisheet 2008—Proceedings of the 7th International Conference and Workshop on Numerical Simulation of 3D Sheet Metal Forming Processes, Interlaken, Switzerland, 2008, pp. 91-95.

[4] M. Luo, T. Wierzbicki, Int. J. Solids Struct. 47 (2010) No. 22, 3084-3102.

[5] M. Li, Y. X. Zhao, X. Hu, S. Huang, J. Shanghai Jiaotong Univ. (Sci.) 45 (2011) 1695-1699.

[6] J. H. Kim, J. H. Sung, K. Piao, R. H. Wagoner, Int. J. Plast. 27 (2011) 1658-1676.

[7] H. G. Gao, L. H. Chen, M. H. Liu, W. T. Yu, Y. F. Wang, J. Iron Steel Res. Int. 18 (2011) Suppl.1-2, 987-989.

[8] AG EDAG, Future Steel Vehicle Phase 2 Overview Report, Future Steel Vehicle Steel Technology, Michigan, USA, 2011.

[9] E. G. Opbroek, Advanced High Strength Steel (AHSS) Application Guidelines, International Iron and Steel Institute committee on Automotive Applications, USA, 2009.

[10] R. B. Song, Q. F. Dai. J. Iron Steel Res. Int. 20 (2013) No. 8, 48-53.

[11] M. Luo, X. Chen, M. F. Shi, H. C. Shih, in: F. Barlat, Y. H. Moon, M. G. Lee (Eds.), NUMIFORM 2010: Proceedings of the 10th International Conference on Numerical Methods in Industrial Forming Processes Dedicated to Professor OC Zienkiewicz (1921—2009), AIP Publishing, Pohang, Republic of Korea, 2010, pp. 455-463.

[12] F. Hayat, H. Uzun, J. Iron Steel Res. Int. 18 (2011) No. 8, 65-72.